Dalton Transactions

Dynamic Article Links

Cite this: *Dalton Trans.*, 2011, **40**, 5984

www.rsc.org/dalton

PAPER

Kojic acid derivatives as powerful chelators for iron(III) and aluminium(III)†

Valeria M. Nurchi,*[a] Joanna I. Lachowicz,[a] Guido Crisponi,[a] Sergio Murgia,[a] Massimiliano Arca,[b] Anna Pintus,[b] Peter Gans,[c] Juan Niclos-Gutierrez,[d] Alicia Domínguez-Martín,[d] Alfonso Castineiras,[e] Maurizio Remelli,[f] Zbigniew Szewczuk[g] and Tadeusz Lis[g]

Received 3rd January 2011, Accepted 30th March 2011
DOI: 10.1039/c1dt00005e

Proceeding from a ligand constituted by two units of kojic acid linked by a methylene group, which proved a very promising chelator for excess iron(III) and aluminium(III) pathologies, two new ligands have been designed and synthesized: one by adding a vanillin molecule in the linker and the second by adding an *o*-vanillin molecule. Both these ligands, on the basis of complex formation studies presented here, show significant potential as therapeutic agents for iron and aluminium overload. Protonation constants of the pure ligands have been determined by potentiometry, and standard reaction heats by calorimetry. Hydrogen bonding plays an important role in the protonation reactions. The crystal structures of both ligands have furthermore been resolved. Complex formation equilibria for the iron complexes have been studied by combined potentiometry–spectrophotometry and those of aluminium by potentiometry alone. All complexes were found to contain two metal ions. NMR diffusion measurements hardly applied to complex formation equilibria and the results of density functional theory (DFT) calculations were powerful tools in confirming the proposed reaction model and in evaluating the relative stabilities of the products. Further support was given by NMR chemical shift measurements and electrospray mass spectrometry.

Introduction

In the last two decades there has been increasing interest in the use of chelation therapy for various medical conditions involving iron.[1,2] Reagents in current use, such as Desferal®, Deferiprone® and Deferasirox®, are based on hydroxamic groups, hydroxy-substituted pyridinones or aromatic ring systems. The design and synthesis of new ligands requires a detailed knowledge of the effect of substituents in the ring and/or attached to the ring upon the stability and redox properties of the complexes formed and the bioavailability of the chelating agent. The redox properties of the complexes are of particular interest in their applications as antioxidants in the context of pathological conditions such as ischemia-reperfusion, or as anti-tumour drugs. Our research has concentrated on the study of the equilibria of complex formation between Fe^{III} and chelating ligands in order to assess the effects of structural and substituent factors.[3–6] The objective has been to design ligands that form complexes with high stability, selectivity, lipophilicity and bioavailability, that is, that satisfy both the chemical requirements and biological constraints for an effective therapeutic agent. Patients receiving dialysis for the treatment of renal insufficiency have in the past been known to suffer from various neurological and bone diseases due to the presence of aluminium in the dialysis water and to the therapy based on aluminium-containing phosphate binders (encephalopathy and osteomalacia). Although the incidence of these problems has been reduced by reducing the aluminium content of dialysis water and avoiding the use of aluminium-containing phosphate binder, the problem is still of great clinical concern.[7] The same chelating agents that are used for iron have also been used to eliminate aluminium from the body. Reagents more specific for aluminium should be developed in view of the different aetiology of aluminium poisoning. Kojic acid (Scheme 1) is related to a pyridinone, but replacement of the ring nitrogen by oxygen results in a weaker chelating agent.[4,8] However, we have found that the compound **1**, which contains two kojic acid residues, forms strong complexes with iron (pFe 23.1) and to a lesser extent with aluminium (pAl 12.8).[8] Because of this and of the ability of that compound to scavenge iron from inside cells,[9] it was thought to be useful to extend the investigation to related compounds in

[a]*Dipartimento di Scienze Chimiche, Cittadella Universitaria, 09042, Monserrato, Cagliari, (Italy). E-mail: nurchi@unica.it; Fax: +39 070 675 4478*
[b]*Dipartimento di Chimica Inorganica e Analitica, Università di Cagliari, Cittadella Universitaria, 09042, Monserrato, Cagliari, Italy*
[c]*Protonic Software, Leeds, U.K.*
[d]*Department of Inorganic Chemistry, Faculty of Pharmacy, Campus Cartuja, University of Granada, E-18071, Granada, Spain*
[e]*Department of Inorganic Chemistry, Faculty of Pharmacy, University of Santiago de Compostela, E-15782, Santiago de Compostela, Spain*
[f]*Dipartimento di Chimica, Università di Ferrara, Via L. Borsari 46, 44121, Ferrara, Italy*
[g]*Faculty of Chemistry, University of Wroclaw, F. Joliot-Curie 14, 50-383, Wroclaw, Poland*
† CCDC reference numbers 801244 and 801245. For crystallographic data in CIF or other electronic format see DOI: 10.1039/c1dt00005e

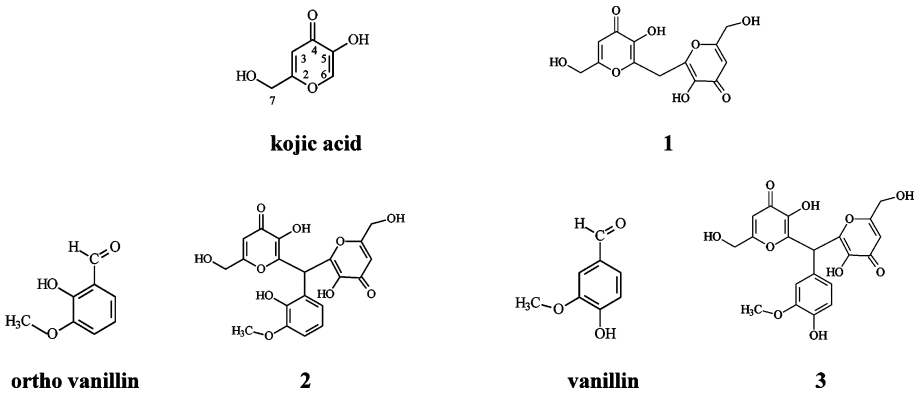

Scheme 1

which different substituents are placed on the linker that joins the two kojic units. The substituents chosen were vanillin and *o*-vanillin, which are different from each other only in the position of the –OH group. That alters the hydrogen bonding ability of the substituent, a factor that determines pFe values.[6] We now present a complete characterization of the acid-base, conformational and structural properties of these new ligands, **2** and **3**, together with the equilibrium constants for the formation of Fe^{III} and Al^{III} complexes.

Experimental

Reagents

HCl, KCl, KOH, D_2O, ethanol, DCl, NaOD, vanillin and *o*-vanillin (purity 99%, used without further purification) were Aldrich products, 5-hydroxy-2-hydroxymethyl-pyran-4-one (kojic acid) and dimethylamine were Fluka products. Carbonate free potassium hydroxide solutions were prepared according to Albert and Serjeant.[10] The new ligands **2** and **3** are shown in Scheme 1. The synthesis of **2**, 2,2′-[(2-hydroxy-3-methoxyphenyl)methanediyl] bis[3-hydroxy-6-(hydroxyl methyl)-4*H*-pyran-4-one] and of **3**, 2,2′-[(4-hydroxy-3-methoxyphenyl)methanediyl]bis[3-hydroxy-6-(hydroxyl methyl)-4*H*-pyran-4-one] were carried out according to Fox and Taylor.[11]

Ligand **2** – Yield 67.1%. Melting point 219 °C. Elemental analysis: $C_{20}H_{18}O_{10} \cdot 0.5H_2O$ (MW 427.36) calculated C 56.21%, H 4.48%, found C 55.71%, H 5.08%. Mass spectrum: LH_4^+ 419.092 (monoisotopic ion), calculated 419.097.

Ligand **3** – Yield 39.0%. Melting point 249 °C. Elemental analysis: $C_{20}H_{18}O_{10}$ (MW 418.35) calculated C 57.42%, H 4.34%, found C 57.61%, H 4.84%. Mass spectrum: LH_4^+ 419.095 (monoisotopic ion), calculated 419.097.

Spectrophotometric–potentiometric measurements

Protonation and complex formation equilibria were studied in a thermostatted glass cell equipped with a magnetic stirrer, a Metrohm LL UNITRODE glass electrode connected to a Metrohm 691 pH-meter, a microburette delivery tube connected to a Dosimat 665 Metrohm titrator, an inlet-outlet tube for Argon and a fibre optic dip probe connected to a Varian Cary 50 UV-vis spectrophotometer. Accuracy and precision of the fibre-optic measurements have been discussed previously.[12] Protonation and Fe^{III} complex formation constants were determined from titration data in which potentiometric and spectrophotometric data were obtained simultaneously. As Al^{III} complexes are colourless, the complex formation constants were determined from potentiometric data alone. Solutions were titrated with 0.1 M KOH at 25.0 °C, and 0.1 M KCl ionic strength. The glass electrode was calibrated daily in terms of hydrogen ion concentration by titration of HCl with KOH under the same experimental conditions. Calibration was performed using the Gran procedure.[13] Ligand concentrations ranged from 2×10^{-4} M to 2.5×10^{-3} M. The complex formation constants were studied using constant ligand concentration and 1 : 1, 1 : 2 and 1 : 3 metal : ligand molar ratios for ligand **2**, and 1 : 1, 1 : 2, 1 : 3 and 2 : 1 for ligand **3**. Potentiometric and spectrophotometric data were processed with hyperquad program.[14] Spectra of pure ligands were recorded in the 200–400 nm spectral range with 0.2 cm path length, while those of Fe^{III} complexes in the 300–700 nm range with 0.5 cm path length. Log β_{pqr} values refer to the overall equilibria $pM + qH + rL \rightleftharpoons M_pH_qL_r$ (electrical charges omitted).

NMR measurements

^1H NMR measurements were made on D_2O solutions at 25 °C with a Bruker Avance 300 MHz (7.05 T) spectrometer operating at 300.131 MHz. A standard BVT 3000 variable temperature control unit with an accuracy of ± 0.5 °C was used. The NMR spectra of free ligand and Al^{III}–L solutions (L ~ 0.002 M and Al : L ratios 1 : 1.8 for ligand **2** and 1 : 3 for ligand **3**) were recorded at different pD values. The pD was adjusted by adding DCl or NaOD and calculated as $pD = pH_{[pHmeter\ reading]} + 0.4$.[15] Chemical shifts were referenced to residual solvent signal (4.800 ppm).

Self-diffusion coefficients were determined using a Bruker DIFF30 probe supplied by a Bruker Great 1/40 amplifier that can generate field gradients up to 1.2 Tm^{-1}. The pulse-gradient stimulated echo (PGSTE) sequence was used. Self-diffusion coefficients were obtained by varying the gradient strength (g) while keeping the gradient pulse length (δ) and the gradient pulse intervals constant within each experimental run. The data were fitted according to the Stejskal–Tanner equation[16]

$$I/I_0 = \exp(-Dq^2t)$$

where I and I_0 are the signal intensities in the presence and absence of the applied field gradient respectively, $q = \gamma g \delta$ is the

so-called scattering vector, γ is the gyromagnetic ratio of the observed nucleus, $t = (\Delta - \delta/3)$ is the diffusion time, Δ is the delay time between the encoding and decoding gradients, and D is the self-diffusion coefficient to be determined. Errors on the self-diffusion coefficient measurements are given as standard deviations.

ESI-MS analysis of complexes

Mass spectra were obtained on a Bruker microTOF-Q spectrometer (Bruker Daltonik, Bremen, Germany), equipped with an Apollo II electrospray ionisation source with an ion funnel. The mass spectrometer was operated in the positive ion mode. Instrumental parameters were as follows: scan range m/z 250–2000, dry gas – nitrogen, temperature 200 °C, ion source voltage 4500 V, collision energy 10 eV. Stock solutions of both ligands were prepared in water. The ligands (~ 10^{-4} mM) were incubated with inorganic salts ($AlCl_3$, and $Fe(NO_3)_3 \sim 2 \times 10^{-4}$ mM) for ten hours at room temperature before the experimental measurements. The final pH of the solutions was ~ 4.0. Solutions were infused at a flow rate of 3 mL min^{-1} at room temperature. Each spectrum is an average of more than 100 individual scans. Before each experiment the instrument was calibrated externally with the Tunemix(tm) mixture (Bruker Daltonik, Germany) in the quadratic regression mode. The overall charge of the analysed ion was calculated on the base of distance between isotopic peaks. The formulae of the complexes were determined by application of the Compass Data Analysis (Bruker Daltonik, Germany) program.

Calorimetric measurements

$\Delta H°$ and $\Delta S°$ values for protonation equilibria were obtained from calorimetric titration data, using a Tronac 450 calorimeter fitted with a 3 mL Dewar titration vessel; the titrant solution was added from a 1 mL Hamilton syringe immersed in the thermostatic bath. A warming resistance (about 100 Ω) was used for instrument electric calibration. A thermistor inside the solution was used to detect temperature changes. The accuracy was checked daily by titrating a tris(hydroxy methyl)aminomethane solution partially neutralized with hydrochloric acid. The thermostatic bath was at 25.00 ± 0.02 °C. The completely automated system was managed by a PC *via* Tronac 900 interface. The potential difference at thermistor ends was measured by a digital multimeter FLUKE 8840A. In-house programs, written in BASIC were used for the management of the calorimetric system, data acquisition and for heat correction for non-chemical factors.[17] Sample solutions containing the ligand ~ 1 mM and KCl, to adjust the ionic strength to 0.1 M, were titrated with standard HCl ~ 0.1 M. $\Delta H°$ values were computed from the calorimetric data deriving from 8–10 independent runs (~ 500 data points) by means of the least-squares computer program HypΔH,[18] which minimizes the function: $U = \Sigma w_i(Q_i^o - Q_i^c)^2$, where w_i are statistical weights and Q_i^o, Q_i^c are the experimental and calculated heats, respectively, over n observations. A literature $\Delta H°_w$ value of 56.4 kJ mol^{-1} was used in the calculations.[19] From experimental $\Delta H°$ values, the corresponding $\Delta S°$ values were computed by means of the Gibbs–Helmholtz equation, $-\Delta G° = -\Delta H° + T\Delta S°$, where the free energy variation was calculated by the corresponding cumulative constants (β), given by potentiometry: $-\Delta G° = 2.303\ RT \log \beta$.

Crystal Structure Determination

Crystal structure determination of **2** (hemi-hydrate). A colourless plate crystal of $C_{20}H_{18}O_{10}\cdot 0.5H_2O$ was mounted on a glass fibre and used for data collection. Crystal data were collected at 100(2) K, using a Bruker X8 Kappa APEXII diffractometer. Graphite monochromated MoK(α) radiation ($\lambda = 0.71073$ Å) was used throughout. The data were processed with APEX2[20] and corrected for absorption using SADABS (transmission factors: 1.000–0.956).[21] The structure was solved by direct methods using the program SHELXS-97[22] and refined by full-matrix least-squares techniques against F^2 using SHELXL-97.[23] Positional and anisotropic atomic displacement parameters were refined for all non-hydrogen atoms. Hydrogen atoms were located in difference maps and included as fixed contributions riding on attached atoms with isotropic thermal parameters 1.2 times those of their carrier atoms. One of the alcohol O atoms (O37) showed disorder and was refined with two positions (occupancy factors 0.56/0.44). Criteria of a satisfactory complete analysis were the ratios of "rms" shift to standard deviation less than 0.001 and no significant features in final difference map. Atomic scattering factors were taken from 'International Tables for Crystallography'.[24] Molecular graphics were made with PLATON[25] program. Summary of the crystal data, experimental details and refinement: $C_{20}H_{18}O_{10}\cdot 0.5H_2O$, 100(2) K, Monoclinic system, Space group $C2/c$, $a = 33.2374(10)$, $b = 7.4001(3)$, $c = 15.2959(6)$ Å, $\beta = 93.956(2)°$, $F(000)$ 1784, data/parameters 3649/286, GOF 1.042, final indices R_1 0.033 and wR_2 0.082.

Crystal structure determination of **3**. The crystals of ligand **3** were obtained from hot water. A colourless plate crystal of $C_{20}H_{18}O_{10}$ was mounted on a glass fibre and used for data collection. Crystal data were collected at 85 K on a Xcalibur PX automated diffractometer with Onyx CCD camera and graphite monochromated MoK(α) radiation ($\lambda = 0.71073$ Å). The structure was solved by direct methods using SHELXS-97[22] and refined by full-matrix least-squares techniques against F^2 using SHELXS-97 programs.[23] Positional and anisotropic atomic displacement parameters were refined for all non-hydrogen atoms. Hydrogen atoms were included as fixed contributions riding on attached atoms with U_{iso} values of 1.2 U_{eq}(C) or 1.5 U_{eq}(O) of their carrier atoms. Both $-CH_2OH$ groups are cooperatively disordered and were restrained using SADI commands (occupancy factors 0.56/0.44). Criteria of a satisfactory complete analysis were the ratios of *rms* shift to standard deviation less than 0.001 and no significant features in final difference map. Atomic scattering factors from "International Tables for Crystallography".[24] Molecular graphics from XP program. Summary of the crystal data, experimental details and refinement: $C_{20}H_{18}O_{10}$, Monoclinic system, Space group $P2_1/n$, $a = 8.365(3)$, $b = 13.150(4)$, $c = 16.819(5)$ Å, $\beta = 98.44(5)°$, $F(000)$ 872, data/parameters 6356/304, GOF 1.002, final indices R_1 0.060 and wR_2 0.054. This data is available in the supplementary information.†

Quantum chemical calculation

Theoretical calculations were performed on the ligands **2** and **3** and on the model complexes $[M_2L_2]^{2+}$, $[M_2L_2(H_2O)]^{2+}$, $[M_2L_2(H_2O)(OH)]^{+}$, and $[M_2L_2(H_2O)_2]^{2+}$ (M = Al, Fe and L = **2**) with the Gaussian09 (Rev. A.02) commercial suite of programs[26]

at Density Functional Theory (DFT) level, adopting the PBEPBE functional (combining the gradient corrected correlation functional and the exchange functional by Perdew, Burke and Ernzerhof),[27] along with the long-range corrections (LC) by Hirao and coworkers.[28] Schäfer, Horn, and Ahlrichs double-ζ plus polarization all-electron basis sets[29] were used for all atoms and were extracted from the Basis Set Exchange Database.[30] For each compound, the optimized geometries were verified through the calculations of harmonic vibrational frequencies, computed analytically. Mulliken and natural charges were calculated at the optimized geometries.[31,32] The programs GaussView 5 and Molden 4.8[33] were used to investigate the charge distributions and molecular orbital shapes. All calculations were carried out on a 64 bit E4 workstation equipped with four quad-core AMD Opteron processors and 16 Gb of RAM and running the OpenSuSE 10.3 Linux operating system.

Results and discussion

Protonation equilibria

The values of the protonation constants of the ligands **2** and **3** and their precursors, obtained from potentiometric data, are given in Table 1. The value of 7.20 for vanillin is more than 2 log units less than the value for phenol (9.80).[34] This is mainly due to the presence of the aldehyde substituent on the aromatic ring. The effect of the aldehyde group can be assessed by comparing the log K value with that of 4-hydroxy benzaldehyde (7.38).[35] The effect of the 3-methoxy group, estimated by Swain–Lupton analysis,[37] is to further reduce the value. Similarly, the value of 7.72 for *o*-vanillin is comparable to that of salicylaldehyde (8.14)[36] after correction for the effect of the 3-methoxy group.

The UV absorption spectra below pH 10 of **2** and **3** are very similar to the spectra of **1**, under the same conditions. This shows that the first two protons are lost from the OH group on the pyran rings (derived from kojic acid). The proton of the OH group on the aromatic ring (derived from vanillin) is the most difficult to remove. This is consistent with the fact that the aldehyde group, the cause of the lowering of the log K value of the phenolic hydroxo group in the parent molecule, is no longer present.

Data from ^{1}H NMR spectra support this assignment and also provide evidence for hydrogen-bonding. The spectra of the fully protonated acids, taken at low pH, are shown in Fig. 1. The assignments of each chemical shift is based on the intensity and multiplicity of the signal. The signals from $H_{4'}$ and $H_{6'}$ in **2** could not be assigned unambiguously. The structures of the acids, LH_3, appears to be wholly consistent with the X-ray structures of the solids, discussed below.

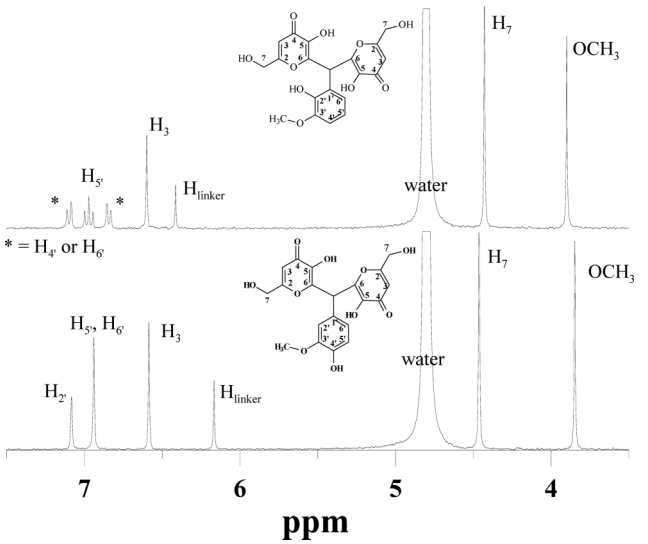

Fig. 1 ^{1}H NMR spectra of ligands **2** (upper) and **3** (lower) at pH 4 and 5 respectively.

Normalised chemical shifts and species concentrations as a function of pH are shown in Fig. 2. The chemical shift of the proton H_3 is effectively constant above pH 10, which confirms that the first two protons are lost from OH groups on the pyran ring, whereas the shifts for $H_{4'}$, $H_{5'}$ and $-OCH_3$ vary most when the third proton is being removed from the hydroxide group on an aromatic ring. The signal from the linker proton shifts to high field while the first proton is being removed, but then shifts to low field as the second and third protons are lost. The shift for the $-CH_2OH$ group moves a little to low field at first and then markedly to high field as the third proton comes away. These observations can be rationalized by postulating the presence of hydrogen bonding, as shown in Scheme 2.

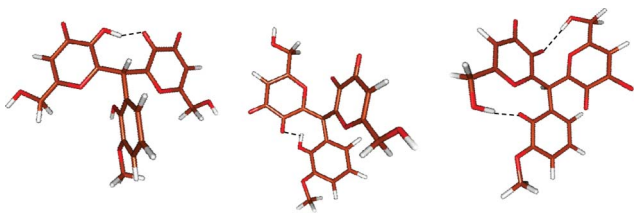

Scheme 2

The formation of hydrogen bonds occurs with a change in the torsional angle at the linker proton, which explains why the chemical shift of that proton does not always change in the same direction with changing pD. When all three protons have been

Table 1 Protonation constants (logK) of the ligands at 25 °C, 0.1 M KCl ionic strength, obtained using Hyperquad program with potentiometric data. Standard deviations on the last figure in brackets

		kojic acid	*o*-vanillin	vanillin	**1**	**2**	**3**
$K_1 = [LH]/[[L][H]^b$	log K_1	7.70 (1)[a]	7.72 (2)	7.20 (1)	9.48 (2)[a]	10.58 (3)	10.18 (2)
$K_2 = [LH_2]/[[LH][H]$	log K_2	—	—	—	6.59 (1)[a]	8.92 (2)	8.84 (1)
$K_3 = [LH_3]/[[LH_2][H]$	log K_3		—	—	—	6.95 (1)	7.21 (1)

[a] Data from reference 8 [b] Electrical charges are omitted for the sake of generality.

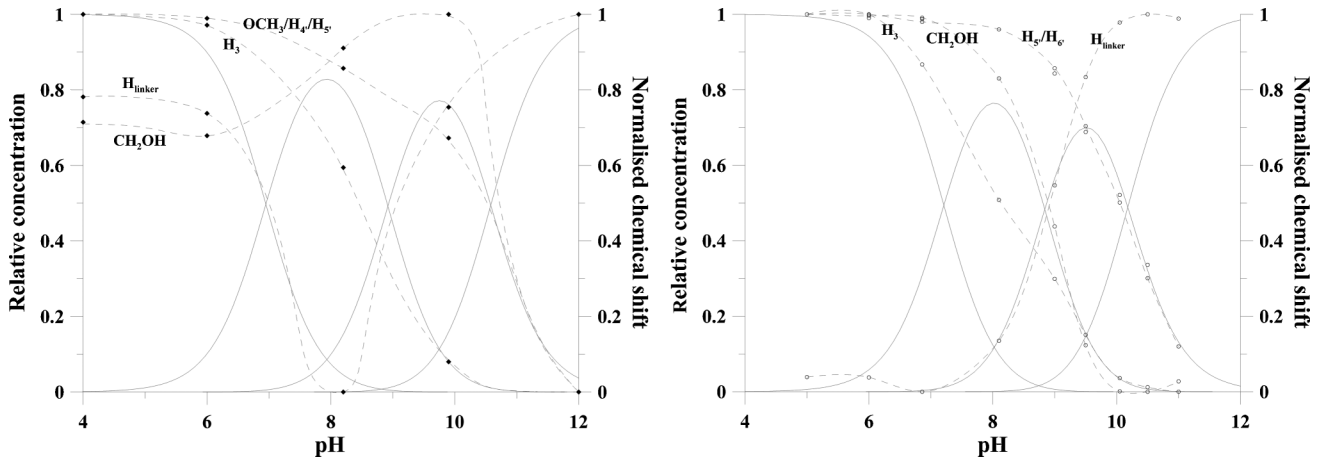

Fig. 2 ^{1}H NMR chemical shifts, normalized to the scale 0–1 (dotted lines), and species concentration as a fraction of the total acid concentration (solid lines) for ligands **2** (left) and **3** (right). The species are, from left to right, LH_3, LH_2^-, LH^{2-}, and L^{3-}.

removed, hydrogen bonds can be formed between the O^- on a pyran ring and the $-CH_2OH$ group, as happens in **1**.

The trends for the protons H_3, $H_{5'}$, $H_{6'}$ and of the methoxy group in **3** are similar to those of **2**. However, hydrogen bonding with the OH group in the *para* position with respect to the ligand attached to the linker is geometrically impossible. In this case a hydrogen bond is formed with the $-CH_2OH$ group after loss of the second proton, as with **1**.

Hydrogen bonding has a noticeable effect on the protonation constants. The log K values for the first proton of the kojic moieties in ligands **1**, **2** and **3**, are 9.48, 8.92 and 8.84, respectively, in spite of the fact that the proton is being added to a phenoxy residue on an identical pyran ring in each case. The log K values for the second proton increase from 6.59 to 6.95 and 7.21.

The standard reaction enthalpies, obtained from calorimetric measurements, and derived entropies are shown in Table 2. In all cases the standard free energy for addition of a proton is mainly determined by the entropy component. Indeed, in ligands **1** and **2**, the standard enthalpy for the first protonation is close to zero; this implies that the enthalpy of protonation of the phenoxide group is approximately equal, but of opposite sign, to the enthalpy of formation of the hydrogen bond(s). With **3**, the spectroscopic evidence has shown that the first proton goes onto the phenoxide group on the vanillin residue, no hydrogen bonds are destroyed in the process and the $-\Delta H^\circ$ value, at 12 ±1 kJ mol^{-1}, is comparable with that of vanillin itself, 16.8 ±0.1 kJ mol^{-1}.

In **2** and **3** $-\Delta H^\circ$ for the third protonation step is a little less than the value for the second protonation step. The $T\Delta S^0$ values show a similar trend. The actual values are comparable to those of kojic acid. By contrast, the values for the first protonation step in **1** and quite different from those of kojic acid which could be due to differences in hydrogen bonding.

Molecular and crystal structures of ligands 2 and 3

Ligand **2** crystallizes in the monoclinic system, space group $C2/c$. The asymmetric unit consists of one acid molecule and half a water molecule. This water molecule is located in a special crystallographic position, according to the hemi-hydrated formula **2**·0.5H_2O (Fig. 3). The atoms of the three rings (two kojic moieties and the *o*-vanillin group) fall in their respective mean planes. Each pair of these planes defines dihedral angles between 70.3° to 83.6°. The molecule seems to be stabilized by three weak intra-molecular H-bonding interactions involving the three –OH phenol-like groups and the corresponding O-acceptors (two keto-kojic and the *o*-vanillin methoxy groups). These interactions build five-membered rings with usual donor–acceptor distances (O25 ··· O26 2.71 Å and O35 ··· O36 2.78 Å for kojic residues, and O12 ··· O13 2.67 Å for the *o*-vanillin arm) but rather low angle

Table 2 Thermodynamic parameters for protonation of the ligands. T = 25 °C, ionic strength = 0.1 M KCl. Standard deviations on the last figure in brackets

Ligand	Definition	log K	$-\Delta G^0$ (kJ mol^{-1})	$-\Delta H^0$ (kJ mol^{-1})	$T\Delta S^0$ (kJ mol^{-1})
2	$K_1 = [LH]/[L][H]$	10.58 (3)	60.4 (2)	0 (1)	60 (1)
	$K_2 = [LH_2]/[LH][H]$	8.92 (2)	50.9 (1)	14 (1)	37 (1)
	$K_3 = [LH_3]/[LH_2][H]$	6.95 (1)	39.6 (1)	12 (2)	28 (2)
3	$K_1 = [LH]/[L][H]$	10.18 (2)	58.1 (3)	12 (1)	46 (1)
	$K_2 = [LH_2]/[LH][H]$	8.84 (1)	50.4 (1)	16 (1)	34 (1)
	$K_3 = [LH_3]/[LH_2][H]$	7.21 (1)	41.1 (1)	12 (1)	29 (1)
Vanillin	$K = [LH]/[L][H]$	7.20 (1)	41.1 (1)	16.8 (1)	24.3 (1)
Kojic acid	$K = [LH]/[L][H]$	7.70 (1)	43.9 (1)	13.0 (1)	30.9 (1)
1[a]	$K_1 = [LH]/[L][H]$	9.48 (2)	54.1 (1)	1.7 (8)	52.4 (8)
	$K_2 = [LH_2]/[LH][H]$	6.59 (1)	37.6 (1)	7 (1)	31 (1)

[a] Data from reference 8

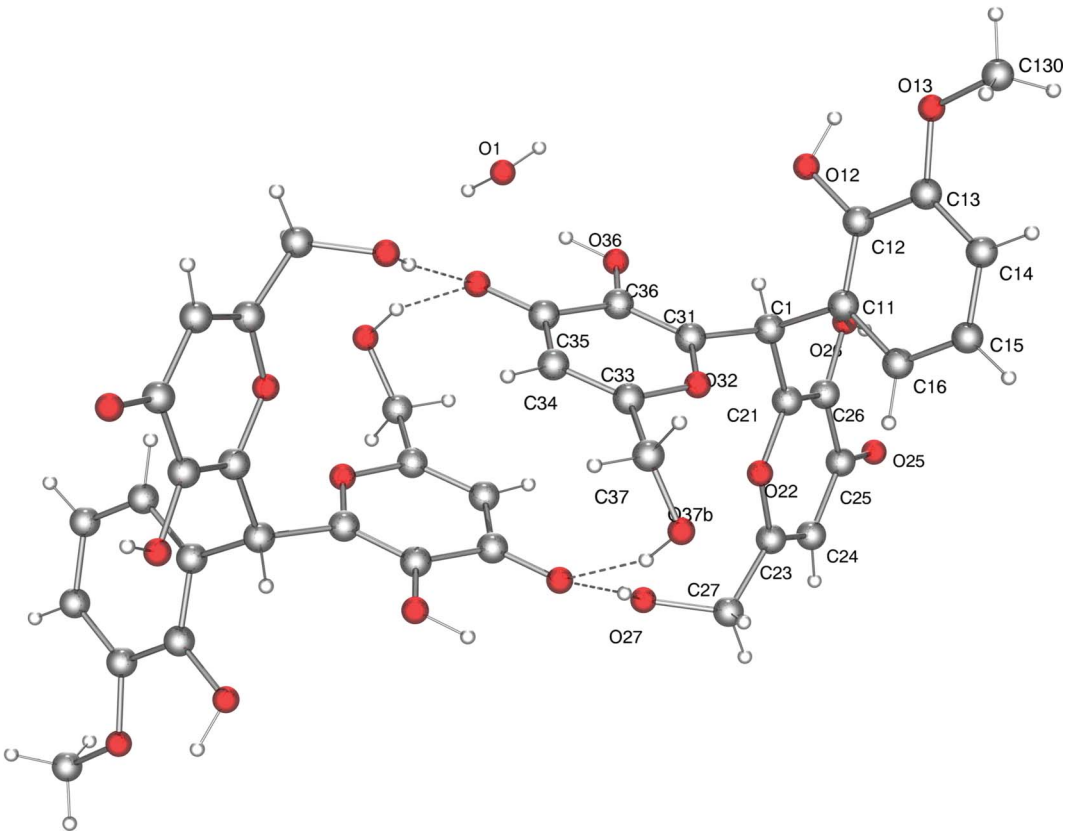

Fig. 3 Pair of H-bonded organic molecules and a water molecule in the crystal of compound **2**. The organic molecules are symmetry related by an inversion transformation. Only one of the two conformational positions in the disordered hydroxyl-methyl arm is showed (-C37–O37B–H372).

values (115.3°, 107.1° and 108.3° respectively). A similar intra-molecular interaction is observed, for example, in the structure of kojic acid (HKj) (2.717 Å and 113.6°; reference code ZZZFMU01 in CSD database).[38] In the crystal, the hydroxyl-methyl arm of one kojic moiety is delocalized in two conformational positions [-C37–O37(A,B)–H(371,372)] but only one of them (-C37–O37B–H372) is plotted in Fig. 3 for clarity. This kind of disorder has been also observed in the own HKj acid as well as for Kj^- ligands in compound $[Ca(HKj)_2(Kj)_2]\cdot 4H_2O$ (MUGHAX in CSD).[39]

The crystal of **2** consists of a 3D H-bonded network. In this array, pairs of organic molecules related by an inversion centre are linked by H-bonding interactions: O27–H27 $\cdots$ O35#2 (2.742(2) Å, 167.4°, symmetry code #2 = –x,–y,–z). These inter-molecular interactions are reinforced by other weaker ones O37-H $\cdots$ O35#2 (in the two different conformational modes). Other relevant crystal packing features are: (a) except for the O26–H bond, all remaining O–H groups act as H-donors for inter-molecular H-bonding interactions with O-keto-kojic or O-water acceptors; (b) Each water molecule is also an H-donor for O27-hydroxy-methyl acceptors of two neighboring organic molecules, symmetry related by the transformation #1 = x,–y+1,–z+0.5; (c) The O-heterocyclic atoms are not involved in H-bonds.

Compound **3** crystallizes in the monoclinic system, space group $P2_1/n$. The asymmetric unit consists of just one acid molecule (Fig. 4) whose structure is very close to that of compound **2**. In **3**, the hydroxyl-methyl arm of both kojic moieties are disordered in two conformational positions [C27(A,B)–O27(A,B)–H(27C,F) and C37(A,B)–O37(A,B)–H(37C,F)]. Only a pair of these conformational possibilities enables one additional intra-molecular H-bonding interaction [O37A–H37C $\cdots$ O27A, 2.842(3) Å, 172.3°],

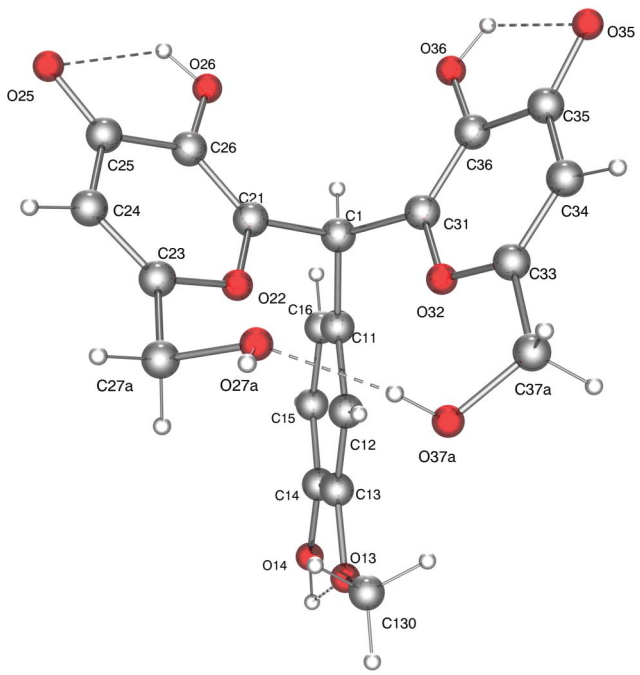

Fig. 4 Asymmetric unit in the crystal of compound **3**. Only the conformation of the $-CH_2OH$ groups involved in an intra-molecular H-bonding interaction between kojic acid moieties is plotted.

shown in Fig. 4. This latter intra-molecular interaction is not observed in the crystal of **2**. Hence, the crystal of **3** can also be defined as a 3D H-bonded network.

The structural differences between **2** and **3** are essentially due to their isomerism. The different position of the –OH group in the vanillin-like arm, as well as the absence of water molecules in crystal **3**, should be highlighted. Both facts lead to: (1) One additional intra-molecular H-bonding interaction in **3** (Fig. 4); (2) Noticeable differences in the relative orientation of the three ligand arms (Fig. 5). This fact is demonstrated by measuring the dihedral angle between them, while in **2** the dihedral angles are 83.58(3)°, 70.32(4)° and 75.95(4)°, in **3** values are 65.53(7)°, 78.58(6)° and 36.05(7)° respectively; (3) The presence of four inter-molecular hydrogen bonds in **3** [O14–H···O27A#1, O26–H···O35#2, O27A–H···O26#4 and O36–H···O25#3 (symmetry codes #1 = x+1/2, –y+3/2, z+1/2, #2 = –x+3/2, y–1/2, –z+1/2, #3 = –x+3/2, y+1/2, –z+1/2 and #4 = x–1, y, z) that replace the two H-bonding interactions corresponding to the water molecule in **2**.

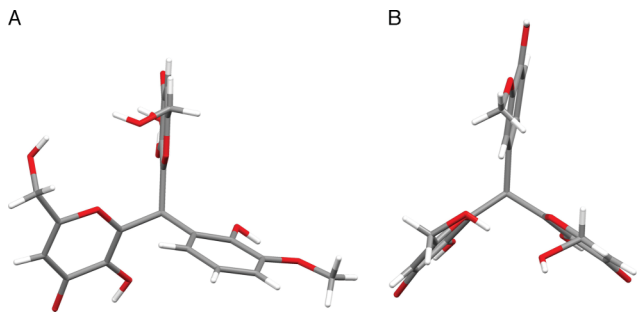

Fig. 5 Comparison of molecular structures of **2** (A) and **3** (B) showing the different orientation of the kojic acid moieties *versus* the vanillin-like ring.

The structural similarities between the organic molecules in the crystals of **2** and **3** do not suggest relevant differences in their protonation constants except for those concerning the *o*-vanillin or *p*-vanillin arms. It is supported by the fact that the mean values between $\log K_2$ and $\log K_3$ are nearly the same for **2** (7.935) and **3** (8.025), whereas the differences $\log K_1 - [(\log K_2 + \log K_3)/2]$ differ significantly (2.645 and 2.155 for **2** and **3** respectively). Likewise, the latter also suggests that overlapping of the protonation between the vanillin-derived arm and the kojic-derived arms is less pronounced for **2** than for **3**. Moreover, $\log K_1 - \log K_2$ and $\log K_2 - \log K_3$ values lower than 4 means a relevant overlapping in successive protonation steps for the full anion forms of the two vanillin-like-bis(kojic) derivatives.

Aluminium complexes

The stability constants for the complexes of ligands **2** and **3** with Al^{III} are given in Table 3. Ligand **2** forms the two dimeric complexes Al_2L_2H and $Al_2L_2H_2$, whereas ligand **3** forms the dinuclear complex Al_2L and the dimers Al_2L_2 and Al_2L_2H. No hydrolyzed species were found for **2** and **3**, in contrast to **1** which forms dimeric hydrolyzed species.[8] Considering the values of the protonation constants for the equilibria $M_2L_2 + H \rightleftharpoons M_2L_2H$ and $M_2L_2H + H \rightleftharpoons M_2L_2H_2$ (Table 4), the species with stoichiometry Al_2L_2 and Al_2L_2H should be chemically formulated as hydrolyzed species $Al_2(LH)_2(OH)_2$ and $Al_2(LH)_2(OH)$, with hydroxide groups bound to aluminium and protonated groups on the vanillin residue. Such hydroxo-bridge aggregates are common in aluminium complexes, as thoroughly discussed in literature on the basis of potentiometric, NMR, ESI-MS and structural data.[40–43] Calculated speciation plots, as a function of pH, are shown in Fig. 6.

The model selection is supported by ^{1}H NMR spectra and ESI-MS measurements. Separate signals for the protons in the ligands are observed in the ^{1}H NMR spectra due to the slow exchange between the free and complexed forms. The spectra of complexes with both **2** and **3** ligands show a similar pattern in which there is a single signal for H_3 and linker protons, shifted downfield by about 0.4 ppm (**2**) and 0.2 ppm (**3**), and an AB quartet shifted downfield but not resolved in its components for the $–CH_2OH$ protons. All signals from the vanillin residue due to the free ligand are at the same chemical shift as the signals from the complexes, except for the signal from $–OCH_3$ group which is shifted ~ 0.03 ppm downfield in the complexes.

The structures of $Al_2L_2H_r$ (r = 0,1,2) are completely different from those proposed for ligand **1**. The unique signals for ligands **2** and **3** in the bound form are consistent with the structure

Table 3 Complex formation constants, $\log \beta_{pqr}$, for the equilibria $pM + qL + rH \rightleftharpoons M_pL_qH_r$. and pM values. T = 25.0 °C, ionic strength = 0.1 M KCl

				Iron(III)			Aluminium(III)		
Species	**p**	**q**	**r**	**1**	**2**	**3**	**1**	**2**	**3**
MLH	1	1	1	18.1(1)	—	—	—	—	—
ML_2	1	2	0	31.66(6)	—	—	20.52(4)	—	—
ML_2H	1	2	1	—	—	—	28.32(2)	—	—
$ML_2(OH)$[a]	1	2	−1	22.83(5)	—	—	—	—	—
$ML_2(OH)_2$[a]	1	2	−2	13.94(7)	—	—	—	—	—
M_2L	2	1	0	—	26.86(2)	—	—	—	23.8(2)
M_2L_2	2	2	0	38.14(2)	47.43(1)	48.82(3)	30.35(1)	—	40.5(2)
M_2L_2H	2	2	1	—	49.57(2)	—	—	44.3(1)	45.4(1)
$M_2L_2H_2$	2	2	2	—	—	—	—	49.7(2)	—
$M_2L_2(OH)$[a]	2	2	−1	35.05(2)	43.91(2)	45.97(1)	24.90(2)	—	—
$M_2L_2(OH)_2$[a]	2	2	−2	30.37(1)	—	42.29(1)	18.56(3)	—	—
pM				23.1	18.9	22.2	12.8	11.9	13.9

[a] Values are for log β* of the species $M_pL_pH_{-r}$. This is related to the stability constant, β, for the equilibrium $pM + qL + rOH \rightleftharpoons M_pL_q(OH)_r$ by $\log \beta^* = \log \beta - r \log K_w$. The concentration calculated for $M_pL_qH_{-r}$ is identical to that calculated for $M_pL_q(OH)_r$.

Table 4 Stepwise formation constants, log K, derived from cumulative constants reported in Table 3

	Iron(III)			Aluminium(III)		
	1	**2**	**3**	**1**	**2**	**3**
$M_2L_2 + H = M_2L_2H$	—	2.1	—	—	—	4.9
$M_2L_2H + H = M_2L_2H_2$	—	—	—	—	5.4	—
$M_2L_2(OH) + H = M_2L_2$	3.1	3.5	2.9	5.5	—	—
$M_2L_2(OH)_2 + H = M_2L_2(OH)$	4.7	—	3.7	6.3	—	—
$ML_2 + H = ML_2H$	—	—	—	7.8	—	—
$ML_2(OH) + H = ML_2$	8.8	—	—	—	—	—
$ML_2(OH)_2 + H = ML_2(OH)$	8.9	—	—	—	—	—

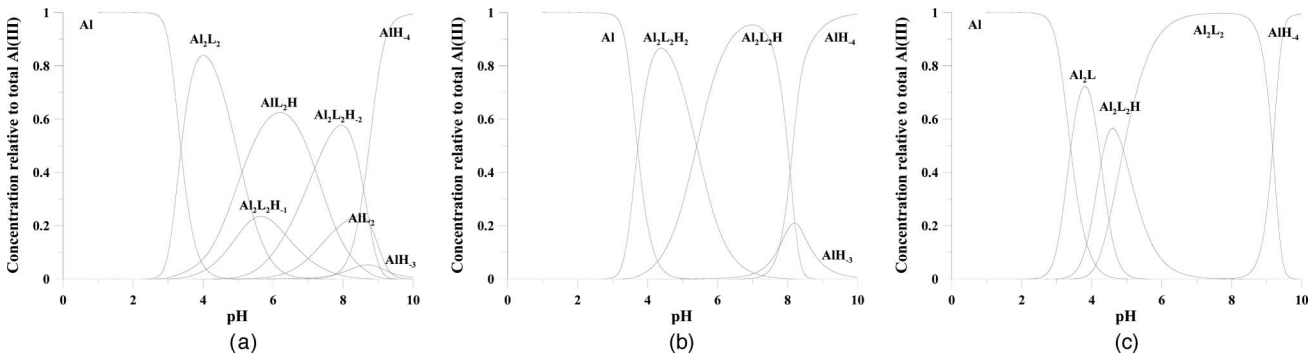

Fig. 6 Distribution curves for the aluminium complexes with the ligands **1** (A), **2** (B), and **3** (C); in all three cases the ligand concentration was 1×10^{-4} M and the Al : L molar ratio was 1 : 2.

reported in Fig. 16 (similar to that previously proposed for the Fe_2L_2 complex[8]) in which each aluminium binds to two phenoxy groups and two ketonic groups from each of the coordinating molecules. This type of aluminium coordination renders the two protons of the $–CH_2OH$ group chemically non-equivalent so that the signal splits into an AB pattern.

The ESI-MS spectrum of Al^{III} complexes with ligand **2**, illustrated in Fig. 7, shows six different species. The major signals, at *m/z* 443.051, 452.057, and 461.062 came from the dinuclear complex with stoichiometry $[Al_2L_2H_2]^{2+}$ and its adducts with water, $[Al_2L_2H_2](H_2O)^{2+}$ and $[Al_2L_2H_2](2H_2O)^{2+}$. Using relatively in-source collision energy (10 eV), some charged hydrates, stable

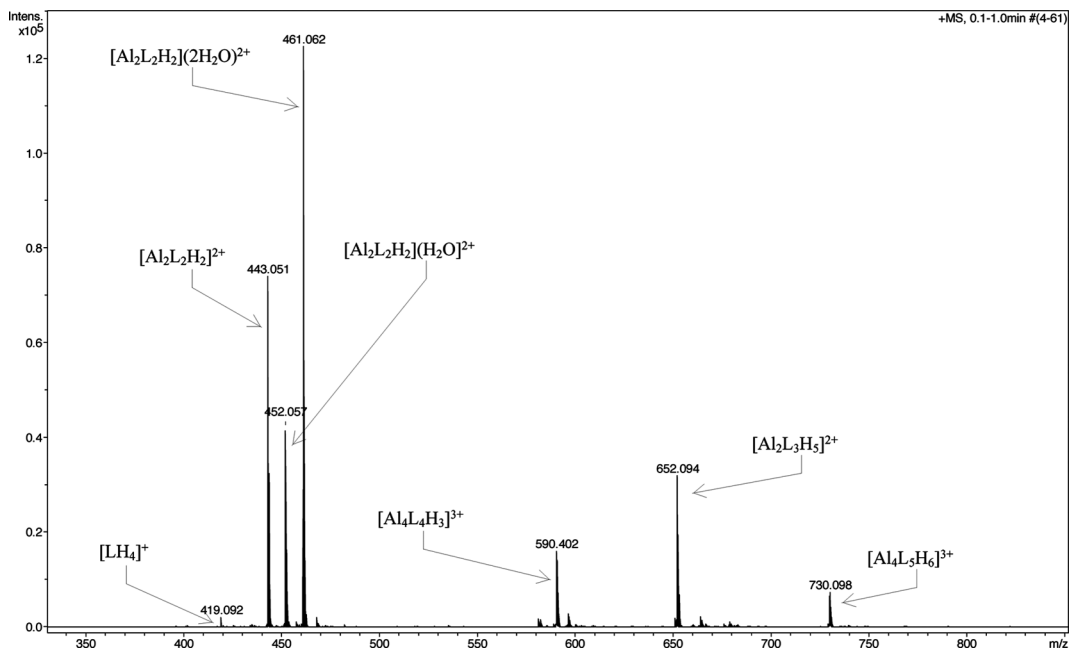

Fig. 7 ESI-MS spectrum of ligand **2** complexed with Al(III) (positive ion mode).

in vacuum, were detected by ESI-MS. Water containing species were not detected if higher cone voltage were used. This fact has often been observed and described in literature.[44] The cone voltage generally has the most profound effect on what complexes and their hydrates are observed in the ESI-MS spectrum. The very strong signal at m/z 461.062 indicate that two water molecules may stabilize the dimeric complex. Three signals at m/z 590.402, 652.094, and 730.098 are assigned to $[Al_4L_4H_3]^{3+}$, $[Al_2L_3H_5]^{2+}$ and $[Al_4L_5H_6]^{3+}$ respectively. The m/z values of the molecular ions are in excellent agreement with the calculated masses. A comparison of the observed and calculated peak intensities is shown Fig. 8.

The ESI-MS spectrum of Al^{III} complexes with ligand **3** is shown in Fig. 9. It is similar to that of Al^{III} complexes with ligand **2**, which indicates the formation of similar complexes. However, the intensity of the peak corresponding to $[Al_2L_3H_5]^{2+}$ at m/z 652.099 is relatively high, indicating that ligand **3** has a higher tendency to form this type of ion.

The self-diffusion coefficient of ligand **3**, (^{L}D) and of Al^{III} in solution, pD = 3.5, ligand to metal ratio 1 : 1, 1×10^{-3} M, (^{AlL}D), was determined through ^{1}H PGSTE NMR experiments, with the aim of discriminating between monomeric and dimeric complexes.[45] The magnitude of the diffusion coefficient is given by the Stokes–Einstein relation,

$D = K_B T/6\pi\eta R_h$, where η is the viscosity of the solvent, T is the temperature, K_B is the Boltzmann constant and R_h represents the hydrodynamic radius of the molecule or molecular aggregate. In principle, this equation is valid only for dilute solutions of non-interacting rigid, spherical molecules. Real molecules perform tumbling motions and are often solvated. Consequently, the radius calculated from the diffusional properties of a molecule gives an

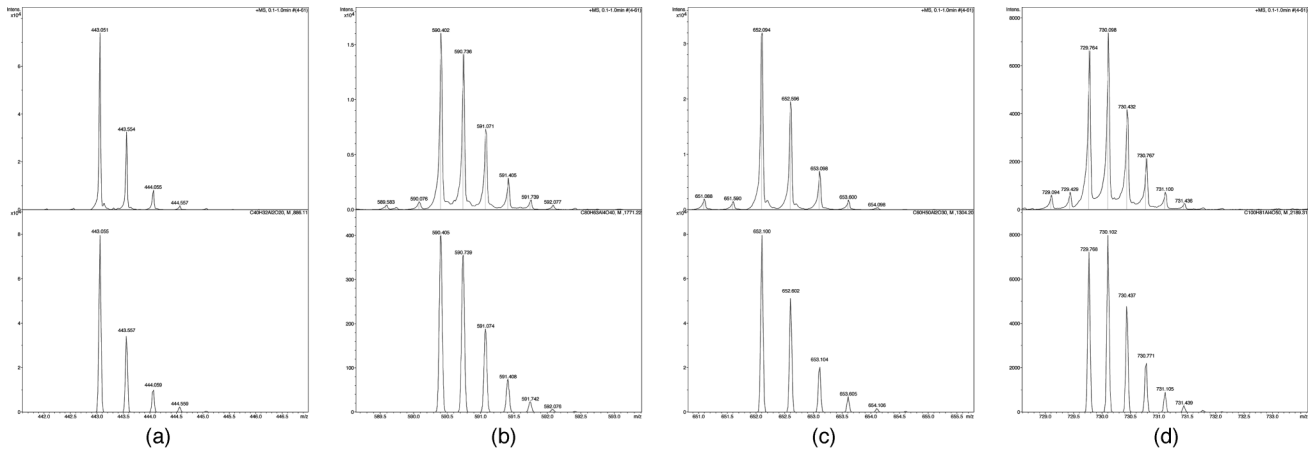

Fig. 8 Comparison of isotopic patterns of the signals for $[Al_2L_2H_2]^{2+}$ (A), $[Al_4L_4H_3]^{3+}$ (B), $[Al_2L_3H_5]^{2+}$ (C), $[Al_4L_5H_6]^{3+}$ (D) from ESI-MS spectrum (upper) with the corresponding calculated ones $[C_{40}H_{32}O_{20}Al_2]^{2+}$ (A), $[C_{80}H_{63}O_{40}Al_4]^{3+}$ (B), $[C_{60}H_{50}O_{30}Al_2]^{2+}$ (C) and $[C_{100}H_{81}O_{50}Al_4]^{3+}$ (D), (bottom).

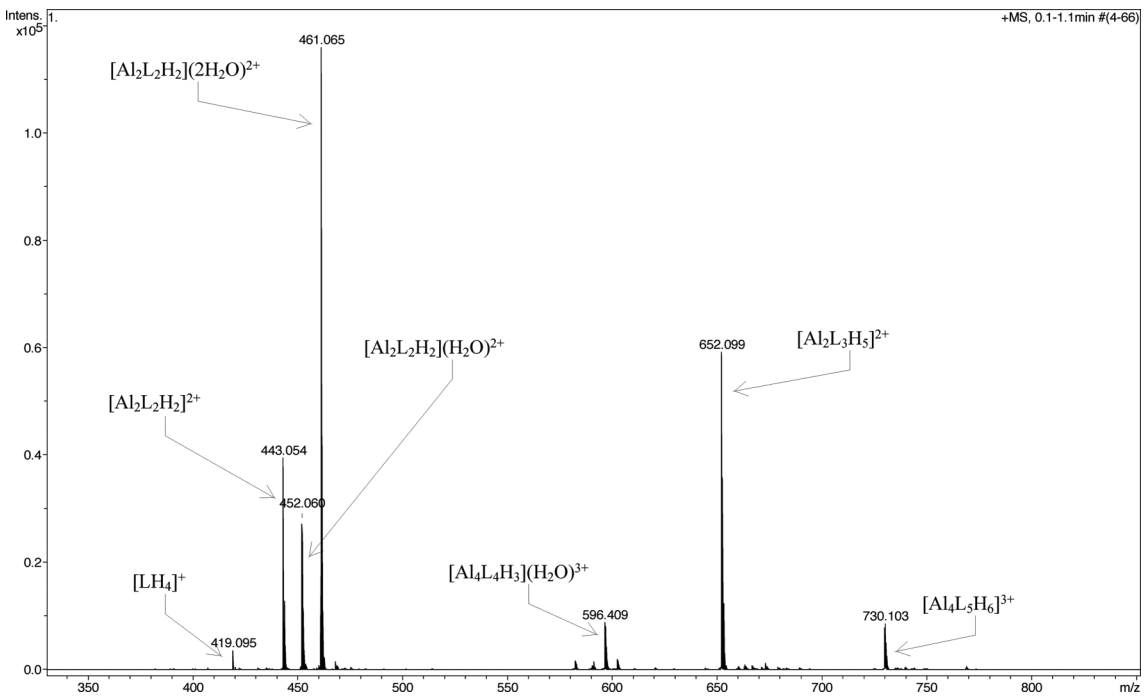

Fig. 9 ESI-MS spectrum of the ligand **3** complexed with Al(III) (positive ion mode).

indication of the *apparent* size of the molecule. Values of ${}^{L}D = 3.7(2)\times10^{-10}$ and ${}^{AlL}D = 2.6(1)\times10^{-10}$ m^2 s^{-1} were obtained: the complex diffuses more slowly than the ligand, as expected in the case of dimer formation. Quantum chemical calculations showed that the ligand closely resembles a sphere with a radius of 5.2 Å. When this value is used in the Stokes–Einstein equation, a D value of 3.7×10^{-10} m^2 s^{-1} is obtained, in excellent agreement with the value observed empirically. Quantum chemical calculations also showed that the Al_2L_2 complex can be described as having the structure of a short rod with a length $l = 19.0$ Å and diameter $d = 7.4$ Å. For dilute short, rigid rods with an axial ratio $p = l/d$ within the range $2 < p < 30$, the following equation was given:[46]

$$D = (K_B T/3\pi\eta l)\,(\ln p + 0.312 + 0.565p^{-1} - 0.100p^{-2})$$

The value of D, calculated on this basis, is 2.96×10^{-10} m^2 s^{-1}. Given the approximations involved, the difference of only 12% between observed and calculated values is strong evidence for the aluminum complex having a dimeric structure.

Fe^{III} complexes

The stability constants for the complexes of ligands **2** and **3** with Fe^{III} are given in Table 3. All complexes are dimers with a general stoichiometry $Fe_2L_2H_r$. When r is negative, the species are actually hydroxo complexes. Calculated speciation plots, as a function of pH, are shown in Fig. 10.

The complex formation equilibria were studied both in strong acidic solutions (pH 0–2) on sets of solutions at different concentrations of HCl, and in the pH range 2–10. Simultaneous fitting of the potentiometric and spectrophotometric data gave the stability constants shown in Table 3.

The stepwise formation constants given in Table 2 indicate that the protonation equilibria involve protons of coordinated water

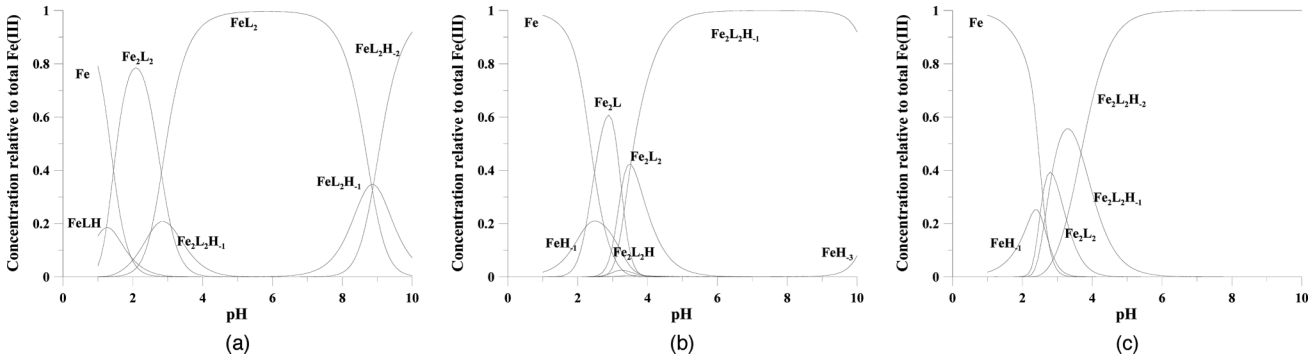

Fig. 10 Distribution curves for the iron complexes with the ligands **1** (a), **2** (b), and **3** (c); in all three cases the ligand concentration was 1×10^{-4} M and the Fe : L molar ratio was 1 : 2.

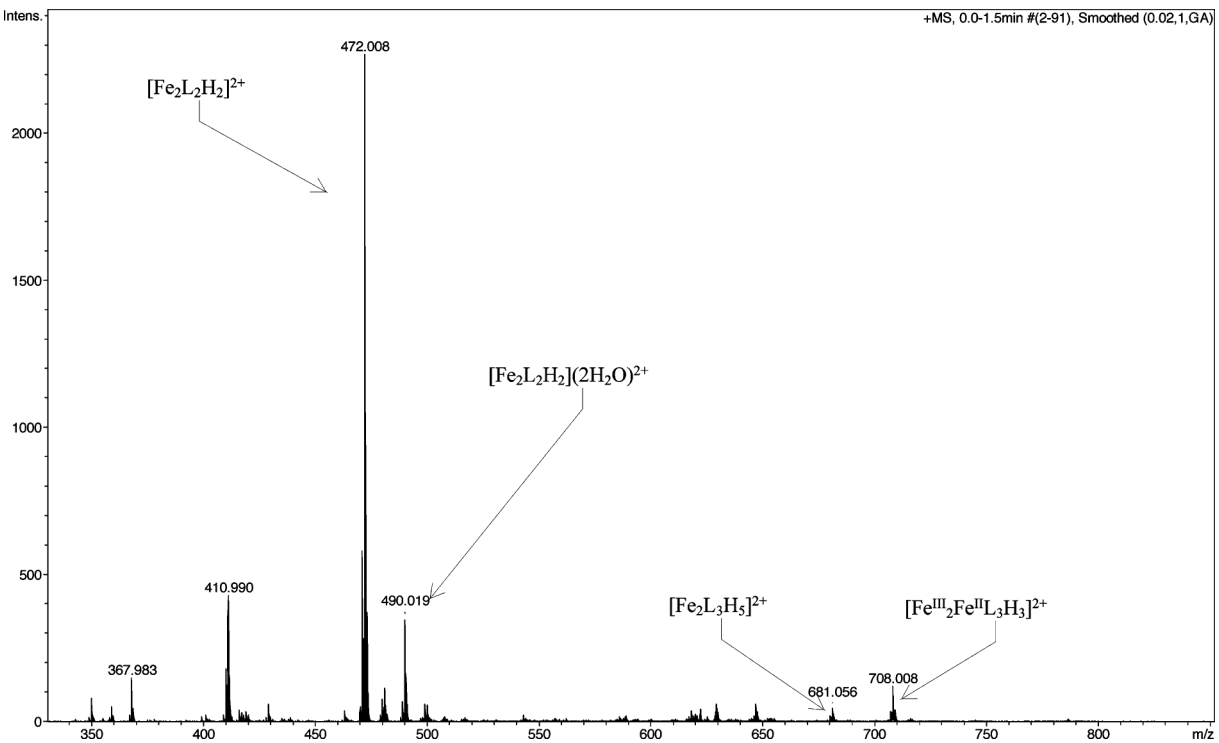

Fig. 11 ESI-MS spectrum of the ligand **2** complexed with Fe(III) (positive ion mode).

molecules. The pK for the OH group on the vanillin residue in the complexes is expected to be very similar to that of the pure ligand, so that protonation of the OH group will occur in the same pH range. Also, the stoichiometry $Fe_2L_2H_{-1}$, is different from the complex formed with ligand **1**. In the latter, the proton is presumably lost from μ-water. This interpretation of hydrolysis is also supported by ESI-MS data.

The ESI-MS spectrum of Fe^{III} complexes with ligand **2** (Fig. 11), shows intense signals at *m/z* 472.008, 490.019, 681.056, and 708.008. These signals were assigned to complexes with the stoichiometry $[Fe_2L_2H_2]^{2+}$, $[Fe_2L_2H_2](2H_2O)^{2+}$, $[Fe_2L_3H_5]^{2+}$ and $[(Fe_3L_3H_3]^{2+}$, respectively. The experimental and simulated ESI-MS spectra, shown in Fig. 12, are in excellent agreement.

The $[Fe_3L_3H_3]^{2+}$ ion must contain two atoms of iron(III) and one of iron(II). This was unexpected since the reaction mixture contained only Fe^{III}. It is well known that reduction processes may occur in the electrospray ionization chamber when operating at the elevated cone voltage. Iron(III), which is relatively easy to reduce, is known to yield a mixture of Fe^{III} and Fe^{II} ions in the ESI-MS experiments.[44] It may be concluded that our results leaded to discovery of new mixed-valence ternary complex $[(Fe^{III})_2Fe^{II}L_3H_3]^{2+}$. Aluminium^{III} cannot be reduced under comparable conditions.

The spectrum obtained from solutions containing complexes of **3** with iron^{III}, shown in Fig. 13, contains four prominent peaks at *m/z* 472.008, 489.008, 680.042, and 708.010, together with a

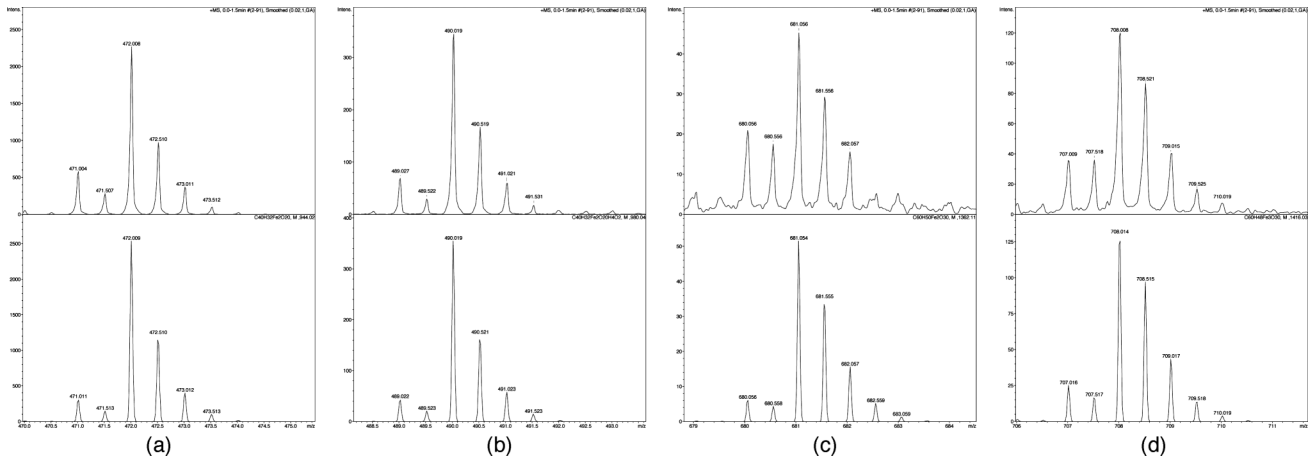

Fig. 12 Comparison of isotopic patterns of the signals for $[Fe_2L_2H_2]^{2+}$ (a), $[Fe_2L_2H_2](2H_2O)^{2+}$ (b), $[Fe_2L_3H_5]^{2+}$ (c), $[Fe^{III}{}_2Fe^{II}L_3H_3]^{2+}$ (d) (upper) with those calculated for $[C_{40}H_{32}O_{20}Fe_2]^{2+}$ (a), $[C_{40}H_{36}O_{22}Fe_2]^{2+}$ (b), $[C_{60}H_{50}Fe_2O_{30}]^{2+}$ (c) and $[C_{60}H_{48}O_{30}Fe_3]^{2+}$ (d) (bottom).

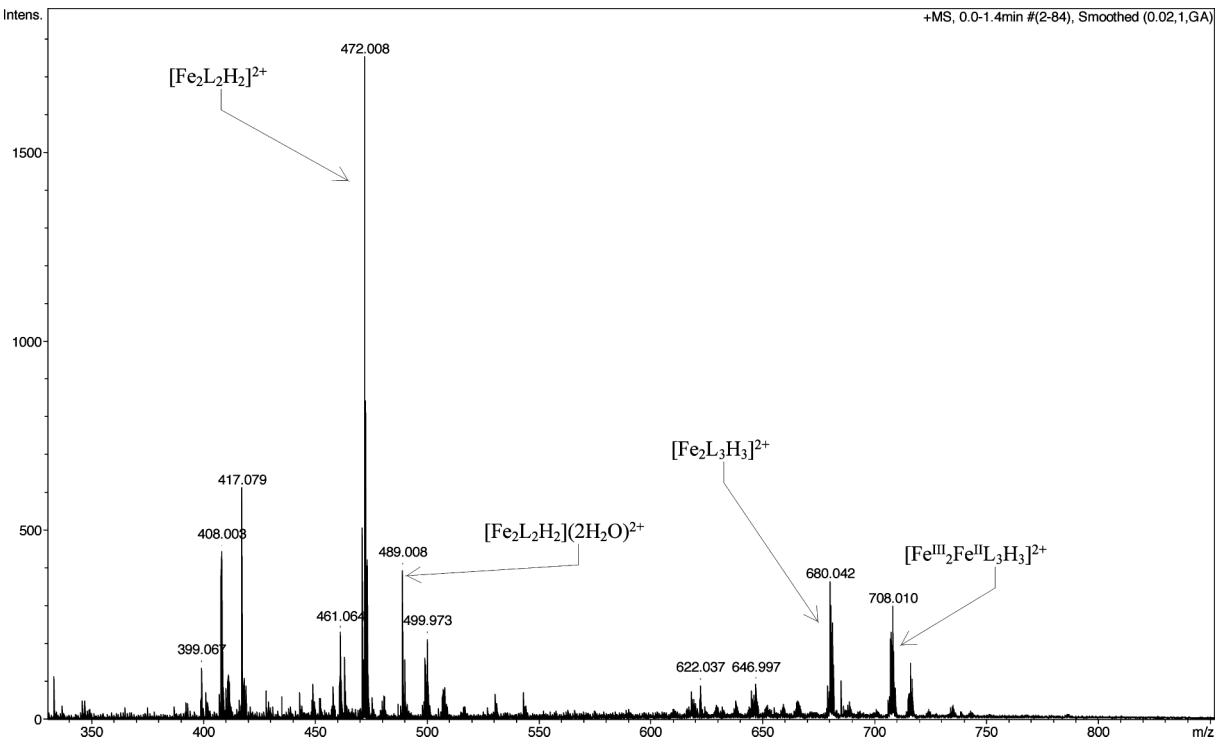

Fig. 13 ESI-MS spectrum of the ligand **3** complexed with Fe(III) (positive ion mode).

number of other unidentified peaks. Three of the prominent peaks are also present in spectrum shown in Fig. 11 and correspond to $[Fe_2L_2H_2]^{2+}$, $[Fe_2L_2H_2](2H_2O)^{2+}$ and $[Fe_3L_3H_5]^{2+}$. The peak at m/z 680.042, however, may not correspond to just $[Fe_2L_3H_5]^{2+}$. Detailed analysis of peaks around m/z 680.042, shown in Fig. 14, suggests existence of a species $[Fe_2L_3H_3]^{2+}$ which may indicate partial oxidation of one ligand **3** molecule in the complex $[Fe_2L_3H_3]^{2+}$. The relatively high intensities of the peaks at m/z 681.048 and 681.550 compared to the simulated isotopic pattern of $[C_{60}H_{48}O_{30}Fe_2]^{2+}$ in Fig. 14 may suggest superposition of the peaks corresponding to $[Fe_2L_3H_3]^{2+}$ and $[Fe_2L_3H_2]^{2+}$ (see Fig. 12C). However the abundance of $[Fe_2L_3H_3]^{2+}$ is significantly higher for ligand **3** (Fig. 14) than that for ligand **2** (Fig. 12C).

Theoretical Calculations

During the past decade, application of density functional theory (DFT) has provided valuable insights into the electronic structure of a wide variety of chemical compounds at an acceptable computational cost.[47] DFT calculations have been carried out on the isolated ligands **2** and **3** (H_3L) and on the dianions (HL^{2-}). The metric parameters of both neutral ligands were in very good agreement with the corresponding structural data obtained by

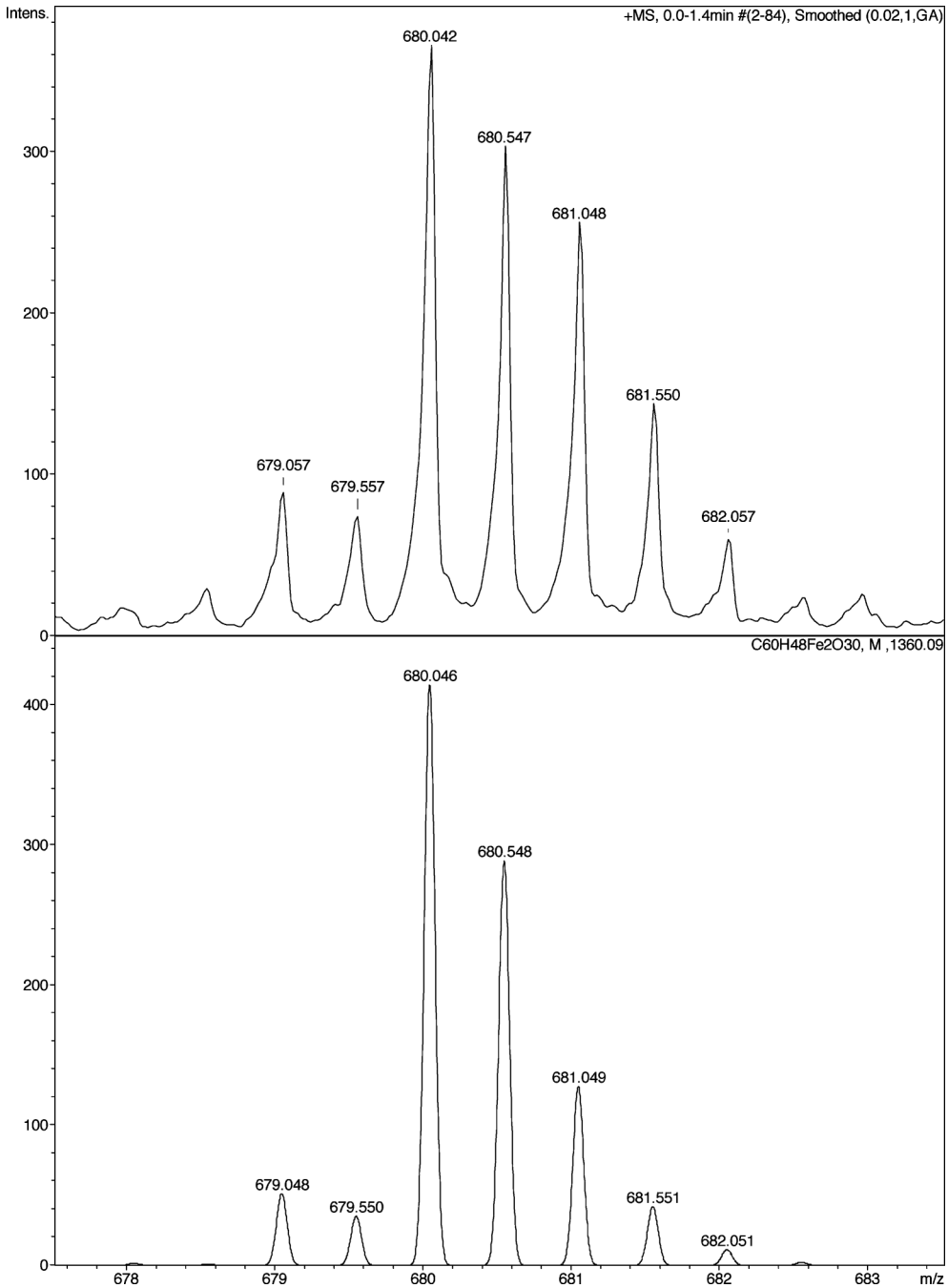

Fig. 14 ESI-MS spectrum of peaks corresponding to $[Fe_2L_3H_3]^{2+}$ (upper). Simulated isotopic pattern of $[C_{60}H_{48}O_{30}Fe_2]^{2+}$ (bottom).

single crystal X-ray diffraction. The experimental C–O bond distances were slightly longer than the calculated ones (calculated average C–O bond distances: 1.218 and 1.321 Å in C═O and C–OH groups, respectively, for ligand **2**; 1.218 and 1.323 Å for H_3L of ligand **3**) because of the network of intermolecular hydrogen bonds present in the crystals. The calculations were extended to the dianionic forms HL^{2-} of both ligands **2** and **3**, obtained by removing the protons on the acidic hydroxy groups of the two kojic residues. Interestingly, in each deprotonated kojic acid unit, the two C–O groups have different bond orders, as shown by the significantly different bond lengths, 1.217 Å compared to 1.240 Å for **2** and 1.218 Å compared to 1.250 Å for **3**. An examination of the highest filled occupied Kohn–Sham (KS) molecular orbitals (MO's) calculated for the dianions (Fig. 15) shows that the HOMO and the HOMO–1 have large contributions from the two oxygen donor atoms of the two kojic residues, which also feature the most negative NBO charges: average values 0.702(6) for **2** and 0.719(8) for **3**.

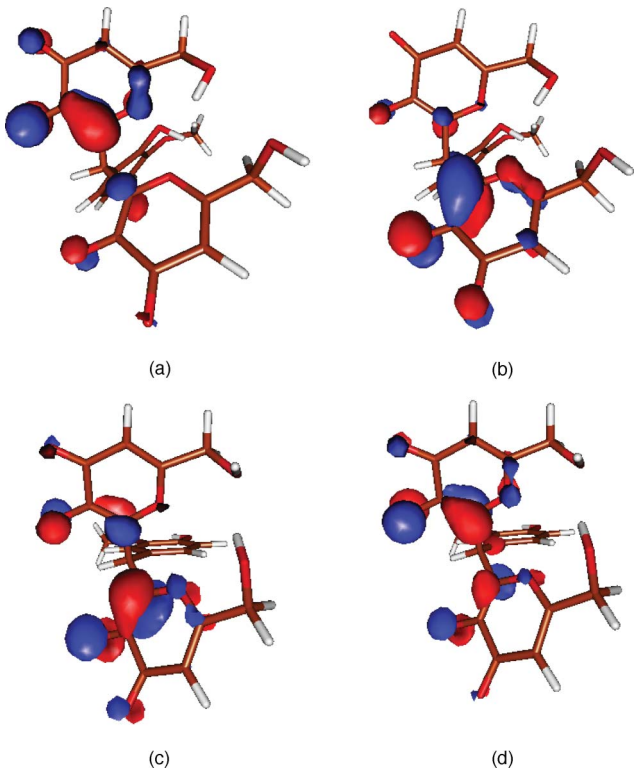

Fig. 15 Drawings of Kohn–Sham HOMO (a, c) and HOMO–1 (b, c) calculated for HL^{2-} for ligand **2** (top) and for ligand **3** (bottom). Contour value 0.05 e.

In the binuclear cation, $[Al_2(HL)_2]^{2+}$, the optimised Al···Al distance was calculated to be 4.699 Å. Each Al^{III} is coordinated tetrahedrally by four oxygen atoms from two deprotonated kojic acid units of different ligands (Fig. 16 left). In each kojic unit, the two optimised C–O distances and the corresponding Al–O are significantly different, with average C–O distances of 1.283(3) and 1.315(1) Å and Al–O distances of 1.798(4) and 1.757(6) Å. Hydrated forms of the complex were optimized by adding one or two water molecules. The optimised structure of the complex $[Al_2(HL)_2(H_2O)]^{2+}$ features the added water molecule coordinated to a single Al^{III} centre, which has a distorted trigonal bipyramidal geometry. The tetra-coordinated aluminium ion has the same coordination geometry and the metric parameters, as were found in $[Al_2(HL)_2]^{2+}$. The penta-coordinated metal has slightly longer metal–oxygen distances with an average Al–O distance of 1.83(3) Å. The addition of a second water molecule to give the complex $[Al_2(HL)_2(H_2O)_2]^{2+}$ results in a binuclear complex featuring, as expected, two penta-coordinated metal centres with similar patterns of Al–O distances, average 1.82(3) Å. Another isomer was found to be stable. In the optimized structure two water molecules bridge the metal ions with $Al–O_{water}$ distances of 2.282, 2.117, 2.227, and 2.161 Å. The aluminium atoms attain a distorted octahedral environment (Fig. 16 right). The four-membered Al_2O_2 ring in this structure brings the two aluminium atoms much closer together at 3.523 Å.

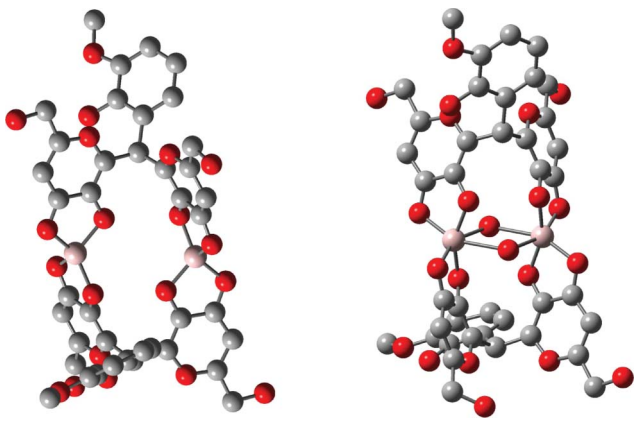

Fig. 16 Optimised molecular structure of the complexes with ligand **2**, $[Al_2(HL)_2]^{2+}$ (left) and $[Al_2(HL)_2(H_2O)_2]^{2+}$ (right). Hydrogen atoms have been omitted for clarity.

A natural population analysis (NPA) shows that on passing from $[Al_2(HL)_2]^{2+}$ to the mono- or di-hydrated forms, the positive charge on aluminium ions is progressively lowered, from 2.06, to 2.03 and 2.02 e in $[Al_2(HL)_2]^{2+}$, $[Al_2(HL)_2(H_2O)]^{2+}$, and $[Al_2(HL)_2(H_2O)_2]^{2+}$, respectively.

When BSSE effects are neglected, analysis of the total electronic energy and formation enthalpy values indicates that the addition of water molecules results in a significant stabilization. Addition of one water molecule to $[Al_2(HL)_2]^{2+}$ provides an extra stabilization enthalpy of 37.1 kcal mol^{-1}. The addition of a second water molecule results in a further stabilization of 22.2 kcal mol^{-1}. The two possible isomers of $[Al_2(HL)_2(H_2O)_2]^{2+}$ differ in their total electronic energy by only 1.3 kcal mol^{-1}. The structure of the hydrolyzed species $[Al_2(HL)_2(H_2O)(OH)]^{+}$ was also optimized with a bridging hydroxo group, a common structural motif in hydrolyzed aluminium species.[48]

For Fe^{III}, the complexes with ligand **2**, $[Fe_2(HL)_2]^{2+}$, $[Fe_2(HL)_2(H_2O)]^{2+}$, and $[Fe_2(HL)_2(H_2O)_2]^{2+}$, related to the species in solution, $[Fe_2(HL)_2]^{2+}$, were optimized. The pattern of bond lengths and charges is similar to that of the aluminium complexes, described above. The addition of one or two water molecules to the complex $[Fe_2(HL)_2]^{2+}$ results in even larger stabilization enthalpy values of 44.7 and 83.2 kcal mol^{-1}.

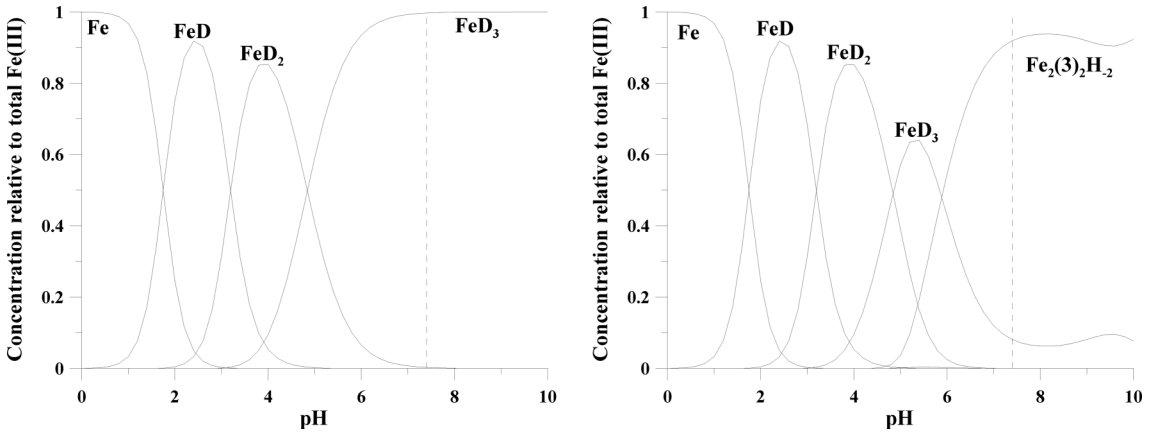

Fig. 17 Speciation curves for the Fe^{III} complexes with Deferiprone (D) in presence of ligands **2** (left) and **3** (right). Fe^{III} concentration was 1×10^{-6} M, Deferiprone 1×10^{-5} M, **2** 1×10^{-5} M and **3** 1×10^{-5} M. The protonation and complex formation constants for the Fe^{III}-Deferiprone system are from Ref. 4.

Conclusions

Two new ligands, which have the potential for use in chelation therapy, have been synthesized and characterized. The rationale for doing this was the recognition that in comparing complexes formed by derivatives of kojic acid and pyridinones, the kojic acid residue is more favourable in terms of structure but less favourable in terms of stability. The new ligands have the same structural advantage and improved chelating properties. The ligands, designated as LH_3, have three ionizable protons. At the physiological pH of 7.4, the species with the highest concentration is LH_2^- (**2**: 72%, **3**: 59%). The species LH_3 also has an appreciable concentration (**2**: 25%, **3**: 38%). The species have a sufficiently low molecular weight, 418 Da, which makes it very likely that, after oral ingestion, they will pass efficiently into the bloodstream through cell membranes. The complex of ligand **2** and Fe^{III} with the highest concentration at pH 7.4 is $[Fe_2L_2(OH)]^-$, and with **3**, $[Fe_2L_2(OH)_2]^{2-}$. This is in marked contrast to the speciation obtained with ligand **1**, for which $[FeL_2]^-$ is the predominant species, though $[Fe_2L_2(OH)]^-$ is also present. The main complexes formed by Al^{III} at this pH are $[Al_2L_2H]^+$ with **2** and $[Al_2L_2]$ with **3**, whereas with ligand **1**, $[AlL_2]^-$ and $[Al_2L_2H_2]$ also have significant concentrations. The found pFe values (18.9 for **2** and 22.2 for **3**), compared with those of the chelators in clinical use, are lower than that for Desferal (26.6),[49] but are comparable with that of Deferiprone (20.7).[4] With the iron scavenging properties of ligands **2** and **3** being similar to those of Deferiprone, their speciation plots in competition with Deferiprone are presented in Fig. 17. These plots show that the 1 : 3 Deferiprone complex FeD_3 is the only species existing at pH 7.4 when ligand **2** is present, while the $Fe_2(\mathbf{3})_2(OH)_2$ complex is the prevailing species in the case of ligand **3**, underlining its efficient competition with Deferiprone.

The found pAl values (11.9 and 13.9 for ligand **2** and **3**, respectively) are lower not only than that of Desferal (19.43),[50] but also than that of Deferiprone (16.1).[51] The ratio pFe : pAl decreases from 1.8 for **1** to 1.6 for **2** and **3**, indicating that ligands **2** and **3** are to some extent better chelators for aluminium than ligand **1**. This can be ascribed to fact that the conformation of aluminium complexes with ligand **1** highly differs from that of complexes with ligands **2** and **3**.

In conclusion, the new ligands show great promise for use in chelation therapy, with ligand **3** being somewhat better at reducing the free iron concentration (higher pFe). They are relatively cheap to produce as the starting materials, kojic acid and vanillin are not expensive. Therefore they merit further examination to determine their capacity to remove iron and/or aluminium from intra-cellular sites where they might have been accumulated in living organisms. Toxicity also needs to be evaluated.

References

1 G. Crisponi and M. Remelli, *Coord. Chem. Rev.*, 2008, **252**, 1225–1240.
2 D. S. Kalinowski and D. R. Richardson, *Pharmacol. Rev.*, 2005, **57**, 547–583.
3 G. Crisponi, V. M. Nurchi and T. Pivetta, *J. Inorg. Biochem.*, 2008, **102**(2), 209–215.
4 V. M. Nurchi, G. Crisponi, T. Pivetta, M. Donatoni and M. Remelli, *J. Inorg. Biochem.*, 2008, **102**(4), 684–692.
5 G. Crisponi, V. M. Nurchi, T. Pivetta, J. Gałęzowska, E. Gumienna-Kontecka, T. Bailly, R. Burgada and H. Kozłowski, *J. Inorg. Biochem.*, 2008, **102**(7), 1486–1494.
6 V. M. Nurchi, T. Pivetta, J. I. Lachowicz and G. Crisponi, *J. Inorg. Biochem.*, 2009, **103**, 227–236.
7 M. A. Santos, *Coord. Chem. Rev.*, 2008, **252**, 1213–1224.
8 V. M. Nurchi, G. Crisponi, J. I. Lachowicz, S. Murgia, T. Pivetta, M. Remelli, A. Rescigno, J. Niclós-Gutíerrez, J. M. González-Pérez, A. Domínguez-Martín, A. Castiñeiras and Z. Szewczuk, *J. Inorg. Biochem.*, 2010, **104**, 560–569.
9 R. C. Fox and P. D. Taylor, *Bioorg. Med. Chem. Lett.*, 1998, 8543–4.
10 A. Albert and E. P. Serjeant, in *The determination of ionization constants: a laboratory manual* (Eds, Chapman and Hall), London, 1984, Ch. 2.
11 R. C. Fox and P. D. Taylor, *Synth. Commun.*, 1998, **28**, 1575–1583.
12 G. Crisponi, A. Caredda, F. Cristiani, A. Diaz, V. M. Nurchi, R. Pinna, T. Pivetta and R. Silvagni, *Ann. Chim.*, 2004, **94**, 147–153.
13 G. Gran, *Analyst*, 1952, **77**, 661–671.
14 P. Gans, A. Sabatini and A. Vacca, *Talanta*, 1996, **43**, 1739–1753.
15 P. K. Glasoe and F. Long, *J. Phys. Chem.*, 1960, **60**, 188–189.
16 E. O. Stejskal and J. E. Tanner, *J. Chem. Phys.*, 1965, **42**, 288–292.
17 L. D. Hansen, T. E. Jensen, S. Mayne, D. J. Eatough, R. M. Izatt and J. J. Christensen, *J. Chem. Thermodyn.*, 1975, **7**, 919–926.
18 P. Gans, A. Sabatini and A. Vacca, *J. Solution Chem.*, 2008, **37**, 467–476.
19 A. Vacca, A. Sabatini and L. Bologni, *J. Chem. Soc., Dalton Trans.*, 1981, 1246–1250.
20 Bruker (2005). *APEX2 Software*, Bruker AXS Inc. V2.0-1, Madison, Wisconsin, USA.

21 G. M. Sheldrick (1997), *SADABS. Program for Empirical Absorption Correction of Area Detector Data*, University of Goettingen, Germany.
22 G. M. Sheldrick, *Acta Crystallogr., Sect. A: Found. Crystallogr.*, 1990, **46A**, 467–473.
23 G. M. Sheldrick (1997), *SHELXL-97, Program for the Refinement of Crystal Structures*, University of Goettingen, Germany.
24 A. J. C. Wilson (1995), *International Tables for Crystallography*, Vol. C, Kluwer Academic Publishers, Dordrecht, The Netherlands.
25 A. L. Spek (2003), *PLATON, A Multipurpose Crystallographic Tool*, Utrecht University, Utrecht, The Netherlands.
26 *Gaussian 09, Revision A02*, M. J. Frisch, G. W. Trucks , H. B. Schlegel, G. E. Scuseria, M. A. Robb, J. R. Cheeseman, G. Scalmani, V. Barone, B. Mennucci, G. A. Petersson, H. Nakatsuji, M. Caricato, X. Li, H. P. Hratchian, A. F. Izmaylov, J. Bloino, G. Zheng, J. L. Sonnenberg, M. Hada, M. Ehara, K. Toyota, R. Fukuda, J. Hasegawa, M. Ishida, T. Nakajima, Y. Honda, O. Kitao, H. Nakai, T. Vreven, J. A. Montgomery, Jr., J. E. Peralta, F. Ogliaro, M. Bearpark, J. J. Heyd, E. Brothers, K. N. Kudin, V. N. Staroverov, R. Kobayashi, J. Normand, K. Raghavachari, A. Rendell, J. C. Burant, S. S. Iyengar, J. Tomasi, M. Cossi, N. Rega, J. M. Millam, M. Klene, J. E. Knox, J. B. Cross, V. Bakken, C. Adamo, J. Jaramillo, R. Gomperts, R. E. Stratmann, O. Yazyev, A. J. Austin, R. Cammi, C. Pomelli, J. W. Ochterski, R. L. Martin, K. Morokuma, V. G. Zakrzewski, G. A. Voth, P. Salvador, J. J. Dannenberg, S. Dapprich, A. D. Daniels, Ö. Farkas, J. B. Foresman, J. V. Ortiz, J. Cioslowski, and D. J. Fox, Gaussian, Inc., Wallingford CT, 2009.
27 J. P. Perdew, K. Burke and M. Ernzerhof, *Phys. Rev. Lett.*, 1996, **77**, 3865–3868; J. P. Perdew, K. Burke and M. Ernzerhof, *Phys. Rev. Lett.*, 1997, **78**, 1396.
28 H. Iikura, T. Tsuneda, T. Yanai and K. Hirao, *J. Chem. Phys.*, 2001, **115**, 3540–3544.
29 A. Schafer, H. Horn and R. Ahlrichs, *J. Chem. Phys.*, 1992, **97**, 2571–2577.
30 D. Feller, *J. Comput. Chem.*, 1996, **17**, 1571–1586; K. L. Schuchardt, B. T. Didier, T. Elsethagen, L. Sun, V. Gurumoorthi, J. Chase, J. Li and T. L. Windus, *J. Chem. Inf. Model.*, 2007, **47**, 1045–1052.
31 NBO Version 3.1, E. D. Glendening, A. E. Reed, J. E. Carpenter, and F. Weinhold.
32 A. E. Reed and F. Weinhold, *J. Chem. Phys.*, 1985, **83**, 1736–40; A. E. Reed, R. B. Weinstock and F. Weinhold, *J. Chem. Phys.*, 1985, **83**, 735–46.
33 G. Schaftenaar and J. H. Noordik, *J. Comput.-Aided Mol. Des.*, 2000, **14**, 123–134.
34 Z. Zwierzchowska-Nowakiwska, *Pol. J. Chem.*, 1986, **60**, 909–768.
35 A. G. Desai and R. M. Milburn, *J. Am. Chem. Soc.*, 1969, **91**, 1958–1961.
36 C. Postmus Jr, L. B. Magnusson and C. A. Craig, *Inorg. Chem.*, 1996, **5**, 1154–1157.
37 G. Crisponi, M. Casu, V. M. Nurchi, F. Cesare-Marincola, T. Pivetta and R. Silvagni, *Talanta*, 2002, **56**, 441–449.
38 J. Lokaj, J. Kozisek, B. Koren, M. Uher and V. Vrabel, *Acta Crystallogr., Sect. A: Found. Crystallogr.*, 1991, **47C**, 193–194.
39 M. Okodo, K. Yamamoto and N. Okabe, *Acta Crystallogr., Sect. A: Found. Crystallogr.*, 2002, **58C**, m469–m470.
40 T. Hedlund and L. O. Ohman, *Acta Chem. Scand., Ser. A*, 1988, **A42**, 702–709.
41 W. Schmitt, P. A. Jordan, R. K. Henderson, G. R. Moore, C. E. Anson and A. K. Powell, *Coord. Chem. Rev.*, 2002, **228**, 115–126.
42 R. Joszai, I. Kerekes, I. Satoshi, K. Sawada, L. Zekany and I. Toth, *Dalton Trans.*, 2006, 3221–3227.
43 M. Tashiro, T. Fujimoto, T. Suzuki, K. Furihata, T. Machinami and E. Yoshimura, *J. Inorg. Biochem.*, 2006, **100**, 201–205.
44 W. Henderson and J. S. McIndoe, in *Mass Spectrometry of Inorganic, Coordination and Organometallic Compounds: Tools - Techniques – Tips*, (Eds, John Wiley & Sons, Ltd.), Chichester, UK, 2005.
45 N. E. Schlörer, E. J. Cabrita and S. Berger, *Angew. Chem., Int. Ed.*, 2002, **41**, 107.
46 L. Galantini and N. V. Pavel, *J. Chem. Phys.*, 2003, **118**, 2865–2872 and references therein.
47 (*a*) W. Koch and M. C. Holthausen, *"A Chemist's Guide to Density Functional Theory'*, 2nd edition, Wiley-VCH, Verlaf GmbH, Weinheim, 2001; (*b*) C. J. Cramer and D. G. Truhal, *Phys. Chem. Chem. Phys.*, 2009, **11**, 10757–10816; (*c*) E. R. Davidson, *Chem. Rev.*, 2000, **100**, 351–352.
48 (*a*) J. B. Parise and C. S. Day, *Acta Crystallogr., Sect. C: Cryst. Struct. Commun.*, 1985, **41**, 515–520; (*b*) J. B. Parise, *Stud. Surf. Sci. Catal.*, 1985, **24**, 271–278; (*c*) E. R. Parnham, P. S. Wheatley and R. E. Morris, *Chem. Commun.*, 2006, 380–382.
49 Z. Hou, K. N. Raymond, B. O'Sullivan and T. W. Esker, *Inorg. Chem.*, 1998, **37**, 6630–6637.
50 M. Gaspar, R. Grazina, A. Bodor, E. Farkas and A. Santos, *J. Chem. Soc., Dalton Trans.*, 1999, 799–806.
51 R. Ma, J. J. Reibenspies and A. E. Martell, *Inorg. Chim. Acta*, 1994, **223**, 21–29.

